An end-to-end generative model for heavy-ion collisions

Jing-An Sun
Institute of Modern Physics
Fudan University
Handan Road 220, Yangpu District, Shanghai, 200433, China

Department of Physics
McGill University
Montreal, Quebec H3A 2T8, Canada
jing-an.sun@mail.mcgill.ca

Abstract

We train a generative diffusion model (DM) to simulate ultra-relativistic heavy-ion collisions from end to end. The model takes initial entropy density profiles as input and produces two-dimensional final particle spectra, successfully reproducing integrated and differential observables. It also captures higher-order fluctuations and correlations. These findings suggest that the generative model has successfully learned the complex relationship between initial conditions and final particle spectra for various shear viscosities, as well as the fluctuations introduced during initial entropy production and hadronization stages, providing an efficient framework for resource-intensive physical goals. The code and trained model are available at https://huggingface.co/Jing-An/DiffHIC/tree/main.

1 Introduction

The heavy-ion collision experiments carried out at the Large Hadron Collider (LHC) and the Relativistic Heavy Ion Collider (RHIC) create a new state of matter, quark-gluon plasma (QGP) [1–3]. However, the QGP cannot be detected directly because of the ultra-short lifetime($\sim 10^{-23}$s) and the microscopic size ($\sim 10^{-14}$m). One must resort to the theoretical model of the heavy-ion collisions and match the experimental observables to infer the properties of the QGP [4, 5]. For this purpose, multistage models have been developed [6–14] that consist of several stages including the initial entropy production [15–24], viscous relativistic hydrodynamic evolution [25–31], and relativistic hadronic transport [32–35].

Despite this success, the traditional numerical simulations of hydrodynamics struggle to confront recent high-precision measurements. In experiments, the data from $10^9 \sim 10^{10}$ collision events [36, 37] allow one to probe the finer details in the system, such as the nuclear structure [38–41] and speed of sound in QGP [42–45], via statistics-demanding observables. It is quite challenging for theoretical model calculations to achieve comparable precision, as the traditional numerical simulation of hydrodynamics for one central event typically takes approximately 120 minutes (10^4 seconds) on a single CPU. As heavy-ion collision physics enters a high-precision era, theoretical modeling needs to evolve to meet the growing computational demands.

In this paper, we introduce DiffHIC (Diffusion Model for Heavy-Ion Collisions), a novel generative diffusion model developed to generate final state two-dimensional charged particle spectra, based on initial conditions and transport parameters. This marks the first application of a diffusive generative model to the simulation of heavy-ion collisions. By comparing observables derived from particle

Machine Learning and the Physical Sciences Workshop, NeurIPS 2024.

spectra generated by both traditional numerical simulations and our trained generative model, we demonstrate that DiffHIC not only accurately replicates integrated and differential observables but also effectively captures higher-order fluctuations and correlations. These results indicate that DiffHIC successfully learns the intricate mapping from initial entropy density profiles to final particle spectra, governed by a set of nonlinear hydrodynamic and Boltzmann transport equations. While preserving the intricate details of the underlying physical processes, DiffHIC significantly accelerates end-to-end heavy-ion collision simulations. For example, DiffHIC accomplishes one single central collision event in just 10^{-1} seconds on a GeForce GTX 4090 GPU.

Related work Machine learning methods have been utilized to speed up observables calculations [46–48]. In these approaches, specific observables are treated as training targets, which can limit flexibility when incorporating other relevant observables. In contrast, our proposed model, DiffHIC, is designed to generate the final charged particle spectra directly from initial conditions, providing an end-to-end simulation framework. This allows for greater adaptability and more comprehensive exploration of observables without retraining for each new target.

2 The generative diffusion model

The generative diffusion model is composed of two parts, the forward process and the reverse process. In the forward process, the original data distribution is transformed to a known prior by gradually injecting noise, which is governed by stochastic differential equation (SDE) [49],

$$d\boldsymbol{x} = f(\boldsymbol{x}, t)dt + g(t)d\boldsymbol{w}. \tag{1}$$

A corresponding reverse-time SDE [50],

$$d\boldsymbol{x} = [f(\boldsymbol{x}, t) - g(t)^2 \nabla_{\boldsymbol{x}} \log p_t(\boldsymbol{x})]dt + g(t)d\bar{\boldsymbol{w}}, \tag{2}$$

transforms the prior distribution back into the data distribution by gradually removing the noise. Here, $\boldsymbol{w}$ and $\bar{\boldsymbol{w}}$ are both standard Wiener processes, $f(\boldsymbol{x}, t)$ is the drift coefficient of $\boldsymbol{x}(t)$, and $g(t)$ is the diffusion coefficient of $\boldsymbol{x}(t)$. In this work, we take Variance Preserving (VP) SDE [49]. The only unknown term is the score function $\nabla_{\boldsymbol{x}} \log p_t(\boldsymbol{x})$, which is estimated by a noise prediction network $\boldsymbol{\varepsilon}$ with parameter $\boldsymbol{\theta}$. With a trained noise prediction network $\boldsymbol{\varepsilon}_{\boldsymbol{\theta}}$, one can generate the sample from a prior standard normal distribution via the solution of reverse SDE. However, stochasticity is introduced in the SDE solution, which will induce unphysical fluctuations in final particle spectra. Therefore, we consider the corresponding probability flow ordinary differential equations (ODE) [49], which converts the probabilistic models to the deterministic models. Additionally, fast sampling can be performed through the numerical methods of ODE [51–53].

In the context of ultra-relativistic heavy-ion collisions, the final particle spectra are critically influenced by the initial entropy density profiles, as well as by physical parameters such as shear viscosity. Therefore, we train a conditional generative diffusion model that takes these initial entropy density profiles and shear viscosity as conditions to accurately generate the final particle spectra. To incorporate the conditional information $\boldsymbol{y}$ into the generative process, we train such a noise prediction network $\boldsymbol{\varepsilon}_\theta(\boldsymbol{x}_t, \boldsymbol{y}, t)$.

3 The multimessenger of heavy-ion physics

We briefly summarize the hybrid model for heavy-ion collisions. At the initial time τ_0, the entropy production is calculated with the TRENTO model [54], where fluctuations in the positions of the nucleons and the contributed entropy in each nucleon-nucleon collision have been taken into account. The system subsequently undergoes hydrodynamic evolution which is realized by MUSIC [26, 25, 27] with a lattice QCD equation of state. In this work, we focus on the mid-rapidity region where the dynamics can be approximated as effectively (2+1)-dimensional with longitudinal boost-invariance. The bulk viscosity effect is neglected and the ratio of shear viscosity over entropy density is set to be $\eta/s = 0.0, 0.1$, and 0.2. When the local energy density drops to a switching value $\varepsilon_{sw} = 0.18$ GeV/fm^3, the transition from fluid to particles occurs through the Cooper-Frye formula [55, 56]. The particles with well-defined positions and momenta are randomly sampled from each fluid cell individually by using the publicly available iSS sampler iSS. After particlization, UrQMD simulates the Boltzmann transport of all hadrons in the system and considers the rescatterings among hadrons and their excited resonance states, as well as all strong decay processes.

4 The generative diffusion model for the heavy-ion collisions

In this work, we train a generative diffusion model to function as a heavy-ion collision event generator. We carried out (2+1)D minimum bias simulations of Pb-Pb collisions at 5.02 TeV, choosing the shear viscosity η/s to be one of three distinct values: 0.0, 0.1, and 0.2. For each value of η/s, we generate 12,000 pairs of initial entropy density profiles and final particle spectra, corresponding to 12,000 simulated events, as the training dataset. 70% of the total events are used for training and the rest are used for validation.

Algorithm 1 Training DiffHIC

Input: Initial entropy profiles $\boldsymbol{I}$, final particle spectra $\boldsymbol{S}$ pairs, and corresponding shear viscosity η/s, number of diffusion steps T, noise schedule β_t
Repeat
for each training iteration **do**
  Sample pairs $(\boldsymbol{I}, \boldsymbol{S}_0, \eta/s)$ from the true data
  Sample $t \sim \text{Uniform}(\{1, \ldots, T\})$
  Sample $\boldsymbol{\varepsilon}$ from standard normal distribution
  Compute noisy spectra $\boldsymbol{S}_t = \sqrt{\bar{\alpha}_t}\boldsymbol{S}_0 + \sqrt{1-\bar{\alpha}_t}\boldsymbol{\varepsilon}$
  Compute loss $\mathcal{L}_t(\boldsymbol{\theta}) = \|\boldsymbol{\varepsilon} - \boldsymbol{\varepsilon}_{\boldsymbol{\theta}}(\boldsymbol{S}_t, \boldsymbol{I}, t, \eta/s)\|^2$
  Update model parameters θ using gradient descent on $\mathcal{L}_t(\theta)$
end for
Until convergence

We denote the particle spectra as $\boldsymbol{S}_0$ and the initial entropy density profiles as $\boldsymbol{I}$. Considering that the spectra $\boldsymbol{S}_0$ depend on the initial entropy density profiles $\boldsymbol{I}$ and the shear viscosity η/s, we train a conditional reverse diffusion process $p(\boldsymbol{S}_0|\boldsymbol{I}, \eta/s)$ without modifying the forward process. We employ an Unet as the noise-prediction network, denoted as $\boldsymbol{\varepsilon}_\theta(\boldsymbol{S}_t, \boldsymbol{I}, \eta/s, t)$. The initial entropy density profiles and their corresponding particle spectra are concatenated along the channel dimension. The diffusion time step t is embedded using a time-embedding layer, while the shear viscosity η/s is encoded using a label-embedding layer. These two embeddings are subsequently summed. The input particle spectra are perturbed by Gaussian noise, and the noisy spectra at time step t are given by $\boldsymbol{S}_t = \sqrt{\alpha_t}\boldsymbol{S}_0 + \sqrt{1-\alpha_t}\boldsymbol{\varepsilon}$, where $\boldsymbol{\varepsilon}$ denotes Gaussian noise. The training objective is to minimize the mean squared error between the true noise $\boldsymbol{\varepsilon}$ and the predicted noise $\boldsymbol{\varepsilon}_\theta$.

In this model, the total noise steps is $T = 4000$ and we chose a linear noise schedule from $\beta_1 = 0.5 \times 10^{-4}$ to $\beta_T = 0.01$. The batch size is set to 32 and the model is saved when the loss on the validation dataset converges. It typically requires 12GB memory and 30h in a 4090 GPU for training.

5 Results

We use additional 10,000 events to assess the efficacy of DiffHIC by comparing its outputs with numerical simulations, focusing on key experimental observables [1, 3, 4, 2, 29, 57–59]. In heavy-ion collisions, the azimuthal emitted particle distribution can be often written as

$$\frac{1}{2\pi}\frac{d^2N}{p_T dp_T d\phi} = \frac{1}{2\pi}\frac{dN}{p_T dp_T}\left(1 + 2\sum_{n=1}^{\infty} v_n(p_T)\cos[n(\phi - \Psi_n(p_T))]\right), \tag{3}$$

where $v_n(p_T)$ is the n-th order anisotropic flow coefficient and $\Psi_n(p_T)$ is its corresponding flow plane angle. Both are p_T differential. One can also perform Fourier expansion for the p_T integrated spectra,

$$\frac{dN}{d\phi} \propto \left(1 + 2\sum_{n=1}^{\infty} v_n\cos[n(\phi - \Psi_n)]\right), \tag{4}$$

where v_n is the n-th order integrated anisotropic flow and Ψ_n is its corresponding flow plane angle. It won't be a surprise that DiffHIC can precisely reproduce integrated observables, such as v_n, which we detail in the appendix. Here, what we pursue is the nice prediction of correlations and fluctuations among these observables. This aspect is particularly demanding for a generative model but serves as

an excellent evaluating criterion, as it requires precise alignment at the pixel level between the true and generated spectra.

The flow correlations are called normalized mixed harmonic cumulants (nMHC) [60–62], $nMHC(v_n^l, v_m^k)$ representing the $(l+k)$-particle correlations between v_n and v_m. The results in Fig. 1 indicate that DiffHIC accurately predicts the true values for 4-particle correlations. Furthermore, the model aligns well with the truth for 6-particle, and 8-particle correlations under the uncertainties.

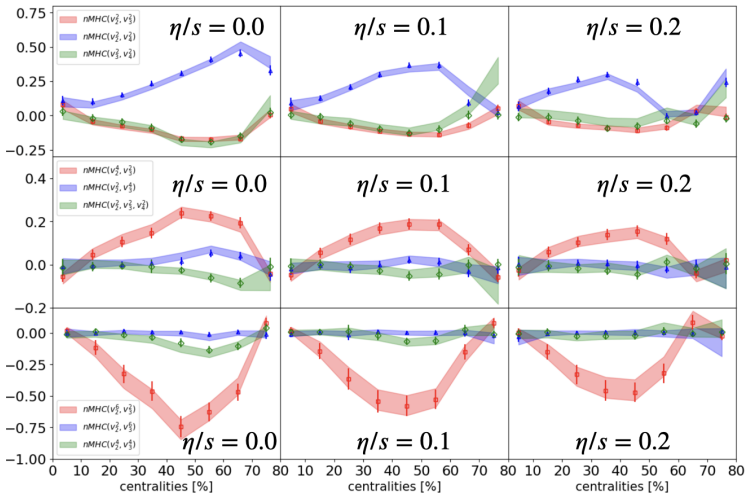

Figure 1: The normalized mixed harmonic cumulants are presented, with open markers indicating the ground truth and colored bands representing the generated results. The first, second, and third rows correspond to the 4-, 6-, and 8-particle cumulants, respectively. The shear viscosity values, from left to right, are $\eta/s = 0.0, 0.1$, and 0.2.

The mean transverse momentum, $\langle p_T \rangle$, serves as a crucial observable, reflecting the temperature of the quark-gluon plasma (QGP). For more nuanced physical investigations, higher-order fluctuations of $\langle p_T \rangle$ are essential [63, 38, 64]. Figure 2 illustrates the centrality dependence of the two-point and three-point correlators, $\langle \delta p_T \delta p_T \rangle$ (left panel) and $\langle \delta p_T \delta p_T \delta p_T \rangle$ (right panel), respectively. The predictions from the trained model are in excellent agreement with the results from numerical simulations.

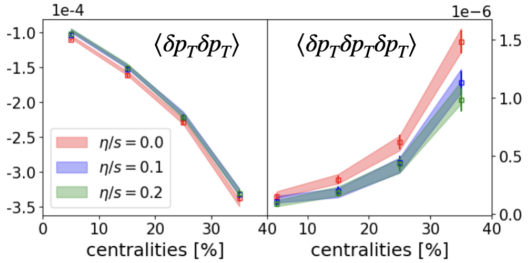

Figure 2: The centrality dependence of 2-particle and 3-particle p_T correlator. The open marks are the ground truth and the color bands are the generated results.

It has been seen that the DiffHIC can capture the observables with surprising precision, even on the fluctuations. Let us focus on the correlations between flow v_n and mean transverse momentum $\langle p_T \rangle$, which have been put forward to constrain the nuclear shape [39–41, 65]. It can be calculated as,

$$\rho_n = \frac{\langle v_n^2 \langle p_T \rangle \rangle - \langle v_n^2 \rangle \langle \langle p_T \rangle \rangle}{\sigma_{v_n^2} \sigma_{\langle p_T \rangle}}, \tag{5}$$

where $\sigma_{v_n^2}, \sigma_{\langle p_T \rangle}$ are the standard variance of v_n^2 and $\langle p_T \rangle$, respectively. As Fig. 3 shows, the trained model accurately reproduces the true ρ_n, making it possible to explore nuclear structure through comprehensive hydrodynamic simulations.

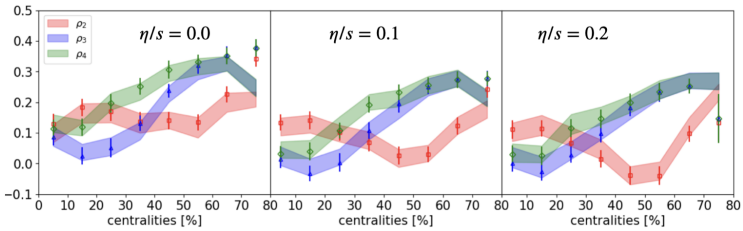

Figure 3: The correlation between flow v_2, v_3, v_4 and mean transverse momentum, with centrality dependence. The open marks represent the ground truth, while the colored lines indicate the generated results. This serves as a crucial probe into nuclear structure. From left to right, the shear viscosity values are $\eta/s = 0.0, 0.1$, and 0.2, respectively.

6 Conclusions and Outlook

In this paper, the state-of-art generative model is for the first time trained to generate the final particle spectra when taking the initial entropy density profiles, named DiffHIC. The trained model can not only predict the integrated and differential observables, such as charged multiplicity, anisotropy flow v_n, and $v_n(p_T)$ $(n = 2, 3, 4)$, but also capture the high-order fluctuations and the correlations among the observables, including the 4-, 6-, and 8-particle flow cumulants, second and third event plane correlations, second and third order $\langle p_T \rangle$ fluctuations, and v_n and $\langle p_T \rangle$ correlations ρ_n $(n = 2, 3, 4)$. Unlike the traditional numerical simulations, including the hydrodynamic evolution and Boltzmann transport, the DiffHIC is an end-to-end model. It speeds up the simulations typically 1,0000 times, relaxing the time and resource concerns. It is as easy as preparing the initial conditions for the time-consuming special physical goals.

Acknowledgments and Disclosure of Funding

The author thanks the hospitality of the nuclear theory group at McGill University, especially for the useful conversations with Charles Gale, Sangyong Jeon, Lipei Du, Xiangyu Wu, and Nicolas Miro Fortier. The computations are made on the Beluga supercomputer system at McGill University, managed by Calcul Quebec and the Digital Research Alliance of Canada.

References

[1] Edward Shuryak. Strongly coupled quark-gluon plasma in heavy ion collisions. *Rev. Mod. Phys.*, 89:035001, 2017.

[2] Jean-Yves Ollitrault. Anisotropy as a signature of transverse collective flow. *Phys. Rev. D*, 46:229–245, 1992.

[3] Ulrich Heinz and Raimond Snellings. Collective flow and viscosity in relativistic heavy-ion collisions. *Ann. Rev. Nucl. Part. Sci.*, 63:123–151, 2013.

[4] B. Alver and G. Roland. Collision geometry fluctuations and triangular flow in heavy-ion collisions. *Phys. Rev. C*, 81:054905, 2010. [Erratum: Phys.Rev.C 82, 039903 (2010)].

[5] Sergei A. Voloshin. Collective phenomena in ultra-relativistic nuclear collisions: anisotropic flow and more. *Prog. Part. Nucl. Phys.*, 67:541–546, 2012.

[6] S. A. Bass and A. Dumitru. Dynamics of hot bulk QCD matter: From the quark gluon plasma to hadronic freezeout. *Phys. Rev. C*, 61:064909, 2000.

[7] Tetsufumi Hirano, Ulrich W. Heinz, Dmitri Kharzeev, Roy Lacey, and Yasushi Nara. Mass ordering of differential elliptic flow and its violation for phi mesons. *Phys. Rev. C*, 77:044909, 2008.

[8] Chiho Nonaka and Steffen A. Bass. Space-time evolution of bulk QCD matter. *Phys. Rev. C*, 75:014902, 2007.

[9] Hannah Petersen, Jan Steinheimer, Gerhard Burau, Marcus Bleicher, and Horst Stöcker. A Fully Integrated Transport Approach to Heavy Ion Reactions with an Intermediate Hydrodynamic Stage. *Phys. Rev. C*, 78:044901, 2008.

[10] Sangwook Ryu, Jean-François Paquet, Chun Shen, Gabriel Denicol, Björn Schenke, Sangyong Jeon, and Charles Gale. Effects of bulk viscosity and hadronic rescattering in heavy ion collisions at energies available at the BNL Relativistic Heavy Ion Collider and at the CERN Large Hadron Collider. *Phys. Rev. C*, 97(3):034910, 2018.

[11] Huichao Song, Steffen A. Bass, and Ulrich Heinz. Viscous QCD matter in a hybrid hydrodynamic+Boltzmann approach. *Phys. Rev. C*, 83:024912, 2011.

[12] Xiangrong Zhu, Fanli Meng, Huichao Song, and Yu-Xin Liu. Hybrid model approach for strange and multistrange hadrons in 2.76A TeV Pb+Pb collisions. *Phys. Rev. C*, 91(3):034904, 2015.

[13] Li Yan. A flow paradigm in heavy-ion collisions. *Chin. Phys. C*, 42(4):042001, 2018.

[14] Chun Shen and Li Yan. Recent development of hydrodynamic modeling in heavy-ion collisions. *Nucl. Sci. Tech.*, 31(12):122, 10 2020.

[15] Joshua Vredevoogd and Scott Pratt. Universal Flow in the First Stage of Relativistic Heavy Ion Collisions. *Phys. Rev. C*, 79:044915, 2009.

[16] Berndt Mueller and Andreas Schaefer. Entropy creation in relativistic heavy ion collisions. *International Journal of Modern Physics E*, 20(11):2235–2267, 2011.

[17] Bjoern Schenke, Prithwish Tribedy, and Raju Venugopalan. Fluctuating Glasma initial conditions and flow in heavy ion collisions. *Phys. Rev. Lett.*, 108:252301, 2012.

[18] Wilke van der Schee, Paul Romatschke, and Scott Pratt. Fully Dynamical Simulation of Central Nuclear Collisions. *Phys. Rev. Lett.*, 111(22):222302, 2013.

[19] Jürgen Berges, Björn Schenke, Sören Schlichting, and Raju Venugopalan. Turbulent thermalization process in high-energy heavy-ion collisions. *Nucl. Phys. A*, 931:348–353, 2014.

[20] Aleksi Kurkela and Egang Lu. Approach to Equilibrium in Weakly Coupled Non-Abelian Plasmas. *Phys. Rev. Lett.*, 113(18):182301, 2014.

[21] Aleksi Kurkela, Aleksas Mazeliauskas, Jean-François Paquet, Sören Schlichting, and Derek Teaney. Effective kinetic description of event-by-event pre-equilibrium dynamics in high-energy heavy-ion collisions. *Phys. Rev. C*, 99(3):034910, 2019.

[22] Aleksi Kurkela, Wilke van der Schee, Urs Achim Wiedemann, and Bin Wu. Early- and Late-Time Behavior of Attractors in Heavy-Ion Collisions. *Phys. Rev. Lett.*, 124(10):102301, 2020.

[23] Aleksi Kurkela, Aleksas Mazeliauskas, Jean-François Paquet, Sören Schlichting, and Derek Teaney. Matching the Nonequilibrium Initial Stage of Heavy Ion Collisions to Hydrodynamics with QCD Kinetic Theory. *Phys. Rev. Lett.*, 122(12):122302, 2019.

[24] Soeren Schlichting and Derek Teaney. The First fm/c of Heavy-Ion Collisions. *Ann. Rev. Nucl. Part. Sci.*, 69:447–476, 2019.

[25] Bjorn Schenke, Sangyong Jeon, and Charles Gale. Elliptic and triangular flow in event-by-event (3+1)D viscous hydrodynamics. *Phys. Rev. Lett.*, 106:042301, 2011.

[26] Bjoern Schenke, Sangyong Jeon, and Charles Gale. (3+1)D hydrodynamic simulation of relativistic heavy-ion collisions. *Phys. Rev. C*, 82:014903, 2010.

[27] Jean-François Paquet, Chun Shen, Gabriel S. Denicol, Matthew Luzum, Björn Schenke, Sangyong Jeon, and Charles Gale. Production of photons in relativistic heavy-ion collisions. *Phys. Rev. C*, 93(4):044906, 2016.

[28] Charles Gale, Jean-François Paquet, Björn Schenke, and Chun Shen. Multimessenger heavy-ion collision physics. *Phys. Rev. C*, 105(1):014909, 2022.

[29] Paul Romatschke. New Developments in Relativistic Viscous Hydrodynamics. *Int. J. Mod. Phys. E*, 19:1–53, 2010.

[30] Wojciech Florkowski, Michal P. Heller, and Michal Spalinski. New theories of relativistic hydrodynamics in the LHC era. *Rept. Prog. Phys.*, 81(4):046001, 2018.

[31] Charles Gale, Sangyong Jeon, and Bjoern Schenke. Hydrodynamic Modeling of Heavy-Ion Collisions. *Int. J. Mod. Phys. A*, 28:1340011, 2013.

[32] J. Weil et al. Particle production and equilibrium properties within a new hadron transport approach for heavy-ion collisions. *Phys. Rev. C*, 94(5):054905, 2016.

[33] S. A. Bass et al. Microscopic models for ultrarelativistic heavy ion collisions. *Prog. Part. Nucl. Phys.*, 41:255–369, 1998.

[34] M. Bleicher et al. Relativistic hadron hadron collisions in the ultrarelativistic quantum molecular dynamics model. *J. Phys. G*, 25:1859–1896, 1999.

[35] Hannah Petersen, Jan Steinheimer, Gerhard Burau, Marcus Bleicher, and Horst Stöcker. A Fully Integrated Transport Approach to Heavy Ion Reactions with an Intermediate Hydrodynamic Stage. *Phys. Rev. C*, 78:044901, 2008.

[36] M. Arslandok et al. Hot QCD White Paper, 3 2023.

[37] S. Acharya et al. The ALICE experiment: a journey through QCD. *Eur. Phys. J. C*, 84(8):813, 2024.

[38] Nicolas Fortier, Sangyong Jeon, and Charles Gale. Comparisons and Predictions for Collisions of deformed ^{238}U nuclei at $\sqrt{s_{NN}} = 193$ GeV, 8 2023.

[39] Jiangyong Jia, Shengli Huang, and Chunjian Zhang. Probing nuclear quadrupole deformation from correlation of elliptic flow and transverse momentum in heavy ion collisions. *Phys. Rev. C*, 105(1):014906, 2022.

[40] Benjamin Bally, Michael Bender, Giuliano Giacalone, and Vittorio Somà. Evidence of the triaxial structure of $^{\mathbf{129}}$Xe at the Large Hadron Collider. *Phys. Rev. Lett.*, 128(8):082301, 2022.

[41] Piotr Bozek. Transverse-momentum–flow correlations in relativistic heavy-ion collisions. *Phys. Rev. C*, 93(4):044908, 2016.

[42] Fernando G. Gardim, Giuliano Giacalone, and Jean-Yves Ollitrault. The mean transverse momentum of ultracentral heavy-ion collisions: A new probe of hydrodynamics. *Phys. Lett. B*, 809:135749, 2020.

[43] Jing-An Sun and Li Yan. Volume effect on the extraction of sound velocity in high-energy nucleus-nucleus collisions, 7 2024.

[44] Aram Hayrapetyan et al. Extracting the speed of sound in the strongly interacting matter created in ultrarelativistic lead-lead collisions at the LHC, 1 2024.

[45] Govert Nijs and Wilke van der Schee. Ultracentral heavy ion collisions, transverse momentum and the equation of state. *Phys. Lett. B*, 853:138636, 2024.

[46] H. Hirvonen, K. J. Eskola, and H. Niemi. Deep learning for flow observables in ultrarelativistic heavy-ion collisions. *Phys. Rev. C*, 108(3):034905, 2023.

[47] Neelkamal Mallick, Suraj Prasad, Aditya Nath Mishra, Raghunath Sahoo, and Gergely Gábor Barnaföldi. Estimating elliptic flow coefficient in heavy ion collisions using deep learning. *Phys. Rev. D*, 105(11):114022, 2022.

[48] Neelkamal Mallick, Suraj Prasad, Aditya Nath Mishra, Raghunath Sahoo, and Gergely Gábor Barnaföldi. Deep learning predicted elliptic flow of identified particles in heavy-ion collisions at the RHIC and LHC energies. *Phys. Rev. D*, 107(9):094001, 2023.

[49] Yang Song, Jascha Sohl-Dickstein, Diederik P Kingma, Abhishek Kumar, Stefano Ermon, and Ben Poole. Score-based generative modeling through stochastic differential equations. In *International Conference on Learning Representations*, 2021.

[50] Brian D.O. Anderson. Reverse-time diffusion equation models. *Stochastic Processes and their Applications*, 12(3):313–326, 1982.

[51] Kaiwen Zheng, Cheng Lu, Jianfei Chen, and Jun Zhu. Dpm-solver-v3: Improved diffusion ode solver with empirical model statistics. In *Thirty-seventh Conference on Neural Information Processing Systems*, 2023.

[52] Cheng Lu, Yuhao Zhou, Fan Bao, Jianfei Chen, Chongxuan Li, and Jun Zhu. DPM-solver: A fast ODE solver for diffusion probabilistic model sampling in around 10 steps. In Alice H. Oh, Alekh Agarwal, Danielle Belgrave, and Kyunghyun Cho, editors, *Advances in Neural Information Processing Systems*, 2022.

[53] Cheng Lu, Yuhao Zhou, Fan Bao, Jianfei Chen, Chongxuan Li, and Jun Zhu. Dpm-solver++: Fast solver for guided sampling of diffusion probabilistic models, 2023.

[54] J. Scott Moreland, Jonah E. Bernhard, and Steffen A. Bass. Alternative ansatz to wounded nucleon and binary collision scaling in high-energy nuclear collisions. *Phys. Rev. C*, 92(1):011901, 2015.

[55] Fred Cooper and Graham Frye. Comment on the Single Particle Distribution in the Hydrodynamic and Statistical Thermodynamic Models of Multiparticle Production. *Phys. Rev. D*, 10:186, 1974.

[56] Pasi Huovinen and Hannah Petersen. Particlization in hybrid models. *Eur. Phys. J. A*, 48:171, 2012.

[57] Derek Teaney and Li Yan. Triangularity and Dipole Asymmetry in Heavy Ion Collisions. *Phys. Rev. C*, 83:064904, 2011.

[58] Derek Teaney and Li Yan. Non linearities in the harmonic spectrum of heavy ion collisions with ideal and viscous hydrodynamics. *Phys. Rev. C*, 86:044908, 2012.

[59] Li Yan and Jean-Yves Ollitrault. Universal fluctuation-driven eccentricities in proton-proton, proton-nucleus and nucleus-nucleus collisions. *Phys. Rev. Lett.*, 112:082301, 2014.

[60] Ming Li, You Zhou, Wenbin Zhao, Baochi Fu, Yawen Mou, and Huichao Song. Investigations on mixed harmonic cumulants in heavy-ion collisions at energies available at the CERN Large Hadron Collider. *Phys. Rev. C*, 104(2):024903, 2021.

[61] Giuliano Giacalone, Li Yan, Jacquelyn Noronha-Hostler, and Jean-Yves Ollitrault. Skewness of elliptic flow fluctuations. *Phys. Rev. C*, 95(1):014913, 2017.

[62] D. Teaney and L. Yan. Event-plane correlations and hydrodynamic simulations of heavy ion collisions. *Phys. Rev. C*, 90(2):024902, 2014.

[63] Somadutta Bhatta, Chunjian Zhang, and Jiangyong Jia. Higher-order transverse momentum fluctuations in heavy-ion collisions. *Phys. Rev. C*, 105(2):024904, 2022.

[64] Giuliano Giacalone, Fernando G. Gardim, Jacquelyn Noronha-Hostler, and Jean-Yves Ollitrault. Skewness of mean transverse momentum fluctuations in heavy-ion collisions. *Phys. Rev. C*, 103(2):024910, 2021.

[65] Björn Schenke, Chun Shen, and Derek Teaney. Transverse momentum fluctuations and their correlation with elliptic flow in nuclear collision. *Phys. Rev. C*, 102(3):034905, 2020.

A supplemental material

A.1 The model parameters used when preparing the datasets

Initial Stage: We choose the most probable values from the Bayesian analysis, $k = 1.0, w = 1.0, p = 0.0$. The norm factors are set to $18.8, 14.4, 5$ for PbPb@5.02TeV, PbPb@2.76Tev, and AuAu@200GeV, respectively. The grid size is $[-15, 15]$ 100*100

Hydrodynamic Stage: We turn off the bulk viscosity during the evolution. The initial time is 0.4 fm. The freezeout energy density is chosen at 0.18 GeV/fm^3. To view the effect of the shear viscosity, we run simulations at three different values, $0.0, 0.1, 0.2$.

Particlization and afterburner: we sample particles at the hyperface untill 100,000 thermal particles are achieved and we use the default set in UrQMD.

A.2 The example of generated charged particle spectra

As good eye illustrations, Fig. 4 and 5 present the typical final particle spectra across all centralities.

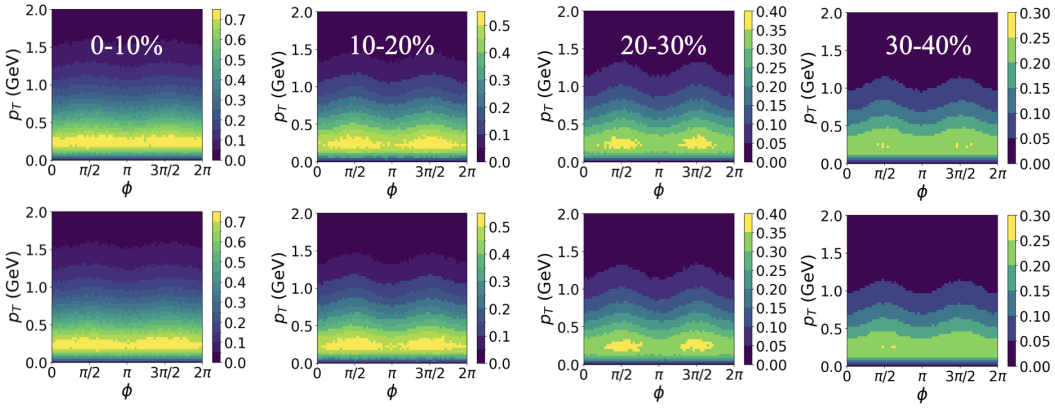

Figure 4: The illustration of generated charged particle spectra, compared to the ground truth, from $0 - 40\%$ centralities. The first row is the ground truth. The second row is the generated spectra.

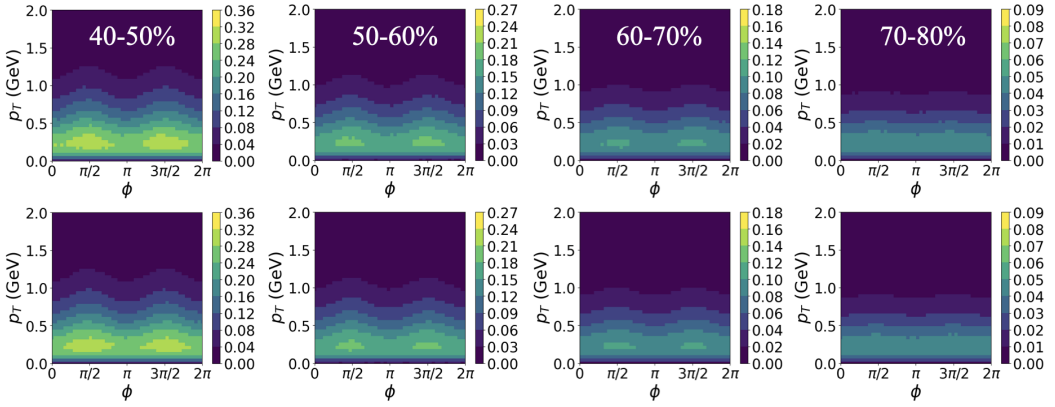

Figure 5: The illustration of generated charged particle spectra, compared to the ground truth, from $40 - 80\%$ centralities. The first row is the ground truth. The second row is the spectra generated.

A.3 The charged particle p_T spectra and the anisotropy flow

We present charged particle transverse momentum spectra $dN/2\pi p_T dp_T$ across all centralities in Fig. 6. It is shown that the model predictions (color lines) perfectly agree with the ground truth

(scatter black points). $dN/2\pi p_T dp_T$ can be interpreted as the zero-order Fourier coefficients in Eq. 3. Before going to the higher order, we first focus on the integrated anisotropy flow v_n defined in Eq. 4. In Fig. 7, the centrality dependence of $v_n, v_n\{2\}$, and $v_n\{4\}$ are shown, from left to the right. From the first to the third row, the $\eta/s = 0.0, 0.1, 0.2$, respectively. We still use the color lines and black points to indicate the generated and true results. We find that the DiffHIC can nicely describe the integrated flow up to $4-th$ order. For the v_2, the 2- and 4-order cumulants can still be captured successfully. However, it is challenging to predict the 4-order cumulants of v_3, v_4, which is easy to understand because higher-order flow and cumulants require more accurate description.

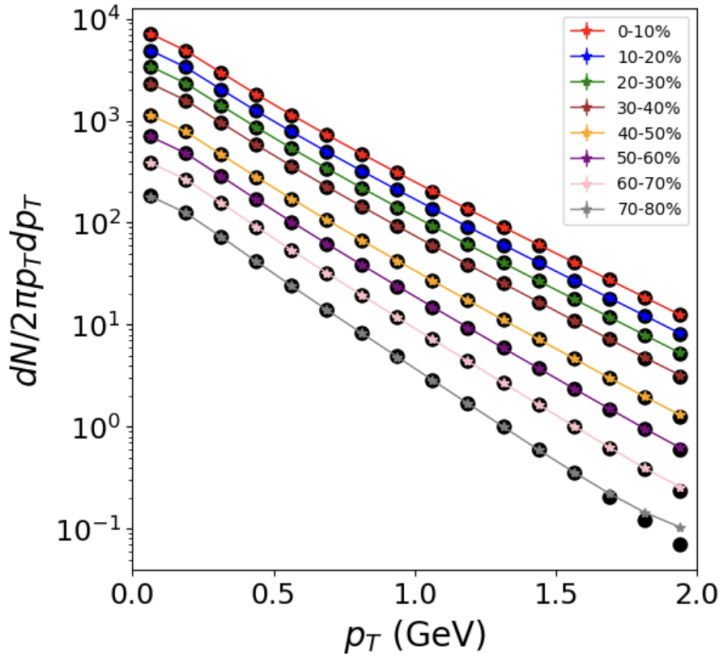

Figure 6: The charged particle transverse momentum spectra. The black points are the ground truth.

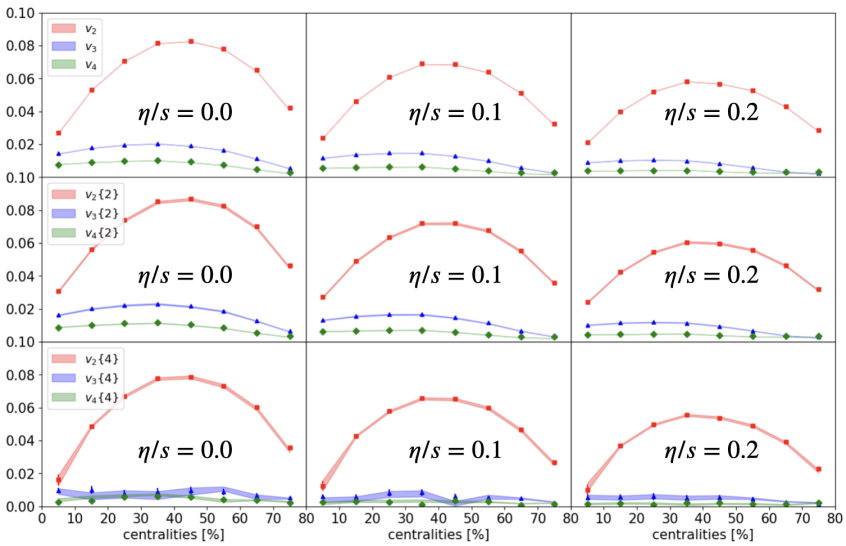

Figure 7: The centrality dependence of integrated anisotropy flow. The black circle points are the ground truth. The first row is the ideal hydrodynamic results. The second and third rows present the results with $\eta/s = 0.1, \eta/s = 0.2$, respectively.

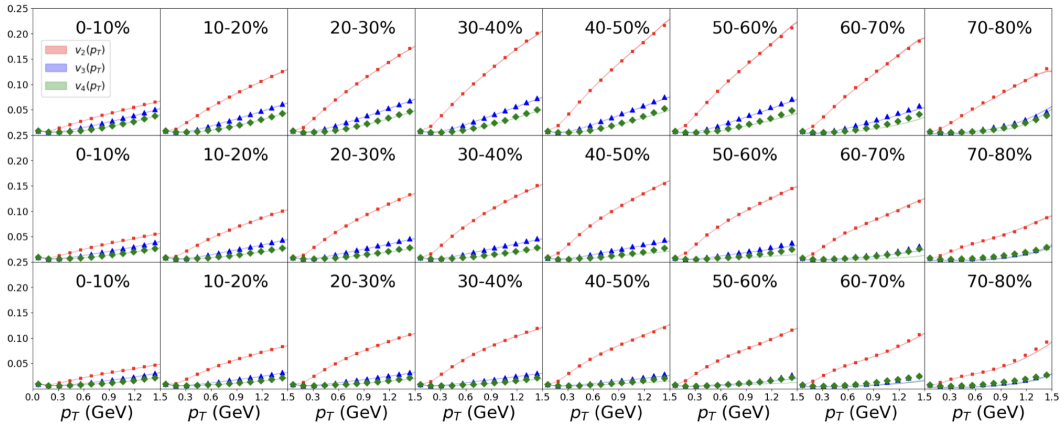

Figure 8: The p_T dependence of integrated anisotropy flow, across all centralities. The black circle points are the ground truth. The first row is the ideal hydrodynamic results. The second and third rows present the results with $\eta/s = 0.1, \eta/s = 0.2$, respectively. In each plot, the red, blue, and green lines represent $v_2(p_T), v_3(p_T)$, and $v_4(p_T)$, respectively.

We next calculate the p_T differential flow $v_n(p_T)$ to evaluate DiffHIC. As Fig. 8 shows, each row presents the $v_n(p_T)$ across all centralities. Again, from the first to the third row, the $\eta/s = 0.0, 0.1, 0.2$, respectively. For the elliptic flow $v_2(p_T)$, it is easy for DiffHIC to get a nice prediction. For higher order flow, there are little discrepancies when $p_T > 1.2$ GeV, and the error is about 4.8% for $v_3(p_T)$ and 9.7% for $v_4(p_T)$.

The 4-particle mixed harmonic cumulants (MHC) are identical to the symmetrical cumulants (SC),

$$MHC(v_n^2, v_m^2) = SC(n, m) = \langle v_n^2 v_m^2 \rangle - \langle v_n^2 \rangle \langle v_m^2 \rangle \tag{6}$$

The 6-particle cumulants are defined as,

$$\begin{aligned}
MHC(v_2^4, v_3^2) &= \langle v_2^4 v_3^2 \rangle - 4\langle v_2^2 v_3^2 \rangle \langle v_2^2 \rangle - \langle v_2^4 \rangle \langle v_3^2 \rangle + 4\langle v_2^2 \rangle^2 \langle v_3^2 \rangle, \\
MHC(v_2^2, v_3^4) &= \langle v_2^2 v_3^4 \rangle - 4\langle v_2^2 v_3^2 \rangle \langle v_3^2 \rangle - \langle v_2^2 \rangle \langle v_3^4 \rangle + 4\langle v_2^2 \rangle \langle v_3^2 \rangle^2, \\
MHC(v_2^2, v_3^2, v_4^2) &= \langle v_2^2 v_3^2 v_4^2 \rangle - \langle v_2^2 v_3^2 \rangle \langle v_4^2 \rangle - \langle v_2^2 v_4^2 \rangle \langle v_3^2 \rangle - \langle v_3^2 v_4^2 \rangle \langle v_2^2 \rangle + 2\langle v_2^2 \rangle \langle v_3^2 \rangle \langle v_4^2 \rangle,
\end{aligned}$$

The 8-particle cumulants are defined as,

$$\begin{aligned}
MHC(v_2^6, v_3^2) &= \langle v_2^6 v_3^2 \rangle - 9\langle v_2^4 v_3^2 \rangle \langle v_2^2 \rangle - \langle v_2^6 \rangle \langle v_3^2 \rangle - 9\langle v_2^4 \rangle \langle v_2^2 v_3^2 \rangle - 36\langle v_2^2 \rangle^3 \langle v_3^2 \rangle \\
&\quad + 18\langle v_2^2 \rangle \langle v_3^2 \rangle \langle v_2^4 \rangle + 36\langle v_2^2 \rangle^2 \langle v_2^2 v_3^2 \rangle \\
MHC(v_2^4, v_4^4) &= \langle v_2^4 v_4^4 \rangle - 4\langle v_2^4 v_2^2 \rangle \langle v_3^2 \rangle - 4\langle v_2^2 v_4^4 \rangle \langle v_2^2 \rangle - \langle v_2^4 \rangle \langle v_4^4 \rangle - 8\langle v_2^2 v_2^2 \rangle^2 - 24\langle v_2^2 \rangle^2 \langle v_3^2 \rangle^2 + 4\langle v_2^2 \rangle \langle v_4^4 \rangle \\
&\quad + 4\langle v_2^4 \rangle \langle v_3^2 \rangle^2 + 32\langle v_2^2 \rangle \langle v_3^2 \rangle \langle v_2^2 v_3^2 \rangle \\
MHC(v_2^2, v_3^6) &= \langle v_2^2 v_3^6 \rangle - 9\langle v_2^2 v_3^4 \rangle \langle v_3^2 \rangle - \langle v_3^6 \rangle \langle v_2^2 \rangle - 9\langle v_3^4 \rangle \langle v_2^2 v_3^2 \rangle - 36\langle v_2^2 \rangle \langle v_3^2 \rangle^3 \\
&\quad + 18\langle v_2^2 \rangle \langle v_3^2 \rangle \langle v_3^4 \rangle + 36\langle v_3^2 \rangle^2 \langle v_2^2 v_3^2 \rangle,
\end{aligned}$$

To eliminate the flow magnitude effect, the heavy-ion community is more interested in the normalized cumulants,

$$nMHC(v_m^k, v_n^l) = \frac{MHC(v_m^k, v_n^l)}{\langle v_m^k \rangle \langle v_n^l \rangle}, \tag{7}$$

$$nMHC(v_m^k, v_n^l, v_p^q) = \frac{MHC(v_m^k, v_n^l, v_p^q)}{\langle v_m^k \rangle \langle v_n^l \rangle \langle v_p^q \rangle}. \tag{8}$$

Now, we focus on the mean transverse momentum and related fluctuation. In a single event, the $\langle p_T \rangle$ is the average transverse momentum of a particle. It reflects the temperature of the QGP. As Fig. 9 shows, it is expected that DiffHIC can perfectly describe such integrated observables.

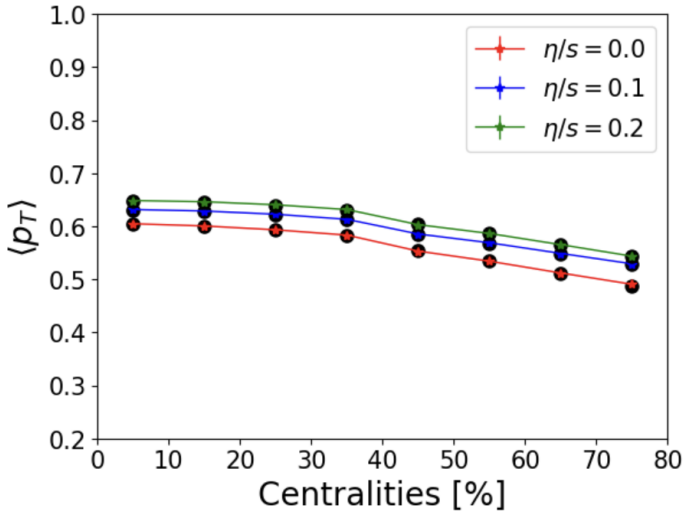

Figure 9: The centrality dependence of mean transverse momentum. The black circle points are the ground truth.

We end this sub-section via the asymmetric cumulants shown in Fig. 10, which not only include the correlations between flows but also the event planes. A good agreement is not a surprise because we have nice predictions on the flow and event plane correlation independently.

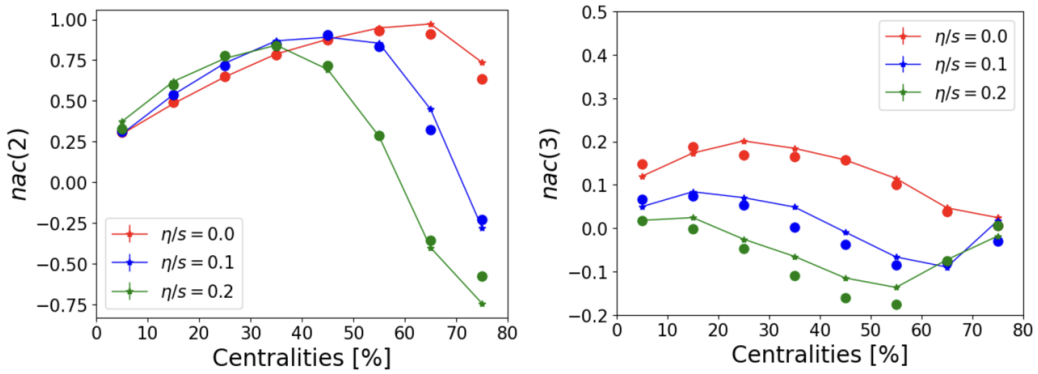

Figure 10: The normalized asymmetric cumulants. The scatter circle points are the ground truth.

The second and third-order p_T correlators are defined as,

$$\langle \delta p_T \delta p_T \rangle = \left\langle \frac{\sum_{i \neq j} (p_i - \langle \langle p_T \rangle \rangle)(p_j - \langle \langle p_T \rangle \rangle)}{N_{ch}(N_{ch} - 1)} \right\rangle_{\text{ev}} \tag{9}$$

$$\langle \delta p_T \delta p_T \delta p_T \rangle = \left\langle \frac{\sum_{i \neq j \neq k} (p_i - \langle \langle p_T \rangle \rangle)(p_j - \langle \langle p_T \rangle \rangle)(p_k - \langle \langle p_T \rangle \rangle)}{N_{ch}(N_{ch} - 1)(N_{ch} - 2)} \right\rangle_{\text{ev}}. \tag{10}$$

In a single event, p_i is the transverse momentum of $i-$th particle. N_{ch} is the total number of charged particles. $\langle \langle p_T \rangle \rangle$ is the event-averaged mean transverse momentum. For efficient computations, in each event, we define

$$Q_n = \sum_{i=1}^{N_{ch}} (p_i)^n. \tag{11}$$

The $\langle p_T \rangle$ and sums over pairs and triplets of particles can be expressed simply in terms of Q_n ($n = 1, 2, 3$):

$$\langle p_T \rangle = \frac{Q_1}{N_{ch}} \tag{12}$$

$$\sum_{i \neq j} p_i p_j = (Q_1)^2 - Q_2, \tag{13}$$

$$\sum_{i \neq j \neq k} p_i p_j p_k = (Q_1)^3 - 3Q_2 Q_1 + 2Q_3. \tag{14}$$

Thus, the correlators can be simplified as,

$$\langle \delta p_T \delta p_T \rangle = \left\langle \frac{Q_1^2 - Q_2}{N_{ch}(N_{ch}-1)} \right\rangle - \left\langle \frac{Q_1}{N_{ch}} \right\rangle^2 \tag{15}$$

$$\langle \delta p_T \delta p_T \delta p_T \rangle = \left\langle \frac{(Q_1)^3 - 3Q_2 Q_1 + 2Q_3}{N_{ch}(N_{ch}-1)(N_{ch}-2)} \right\rangle - 3 \left\langle \frac{(Q_1)^2 - Q_2}{N_{ch}(N_{ch}-1)} \right\rangle \left\langle \frac{Q_1}{N_{ch}} \right\rangle + 2 \left\langle \frac{Q_1}{N_{ch}} \right\rangle^3. \tag{16}$$

The event plane correlations are another important observable in heavy-ion collisions. we plot the different second and third event plane correlations in Fig. 11 respectively.

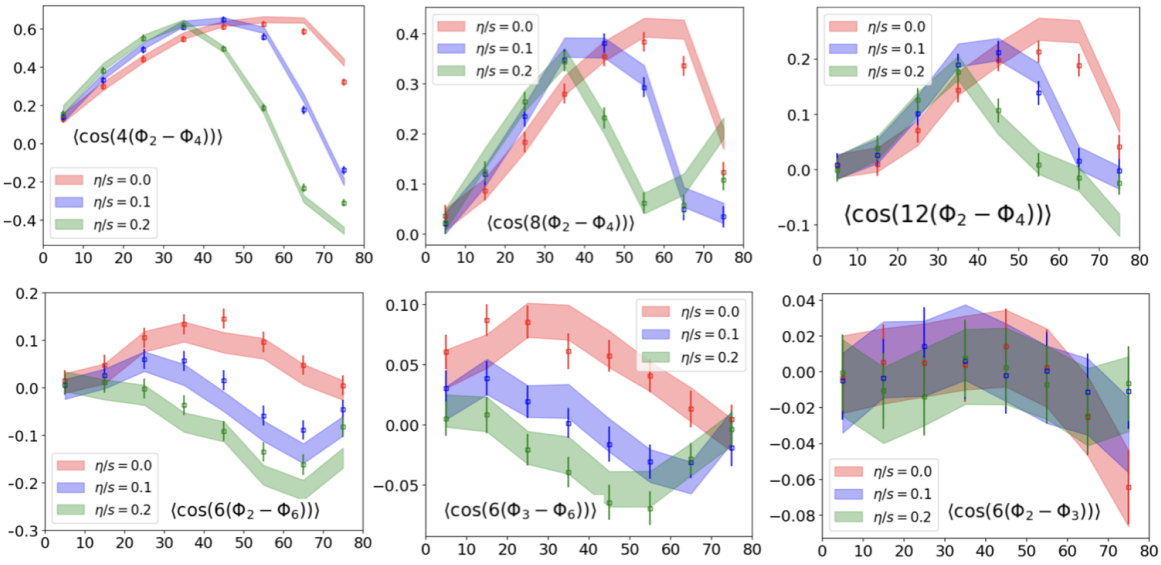

Figure 11: The second event plane correlations. The scatter circle points are the ground truth.